catalysts

MDPI

Article

Terpyridine-Containing Imine-Rich Graphene for the Oxygen Reduction Reaction

Min Seok Lee [1], Mun Ho Yang [1], Jong S. Park [2] and Dong Wook Chang [1,*]

[1] Department of Industrial Chemistry, Pukyong National University, Busan 48547, Korea; lms@pknu.ac.kr (M.S.L.); ymh@pknu.ac.kr (M.H.Y.)

[2] Department of Organic Material Science and Engineering, Pusan National University, Busan 46241, Korea; jongpark@pnu.ac.kr

* Correspondence: dwchang@pknu.ac.kr; Tel.: +82-51-629-6444

Received: 18 October 2017; Accepted: 7 November 2017; Published: 10 November 2017

Abstract: We report a facile synthetic method for the preparation of a terpyridine-containing imine-rich graphene (IrGO-Tpy) using an acid-catalyzed dehydration reaction between graphene oxide (GO) and 4′-(aminophenyl)-2,2′:6′2″-terpyridine. Owing to the presence of terpyridine ligands, cobalt ions (Co^{2+}) were readily incorporated into the IrGO-Tpy structures, affording a metal complex, denoted IrGo-Tpy-Co. Cyclic voltammetry and linear sweep voltammetry measurements confirm the noticeable oxygen reduction reaction (ORR) activities of the IrGo-Tpy and IrGo-Tpy-Co electroacatalysts in alkaline electrolytes, along with the additional merits of high selectivity, excellent long-term durability, and good resistance to methanol crossover. In addition, a remarkable improvement in the ORR performance was observed for IrGO-Tpy-Co compared with that of IrGo-Tpy, arising from the significant contribution of the cobalt-terpyridine complex in facilitating the ORR process.

Keywords: terpyridine; imine-rich graphene; oxygen reduction reaction; electrocatalyst; cobalt-terpyridine complex

1. Introduction

Given the rising global energy demand and various environmental problems, the development of clean and sustainable energy resources has attracted great interest in both academia and industry. Above all, fuel cell technology has become popular because of its advantages such as high energy conversion efficiency, lack of pollutant emission, long life cycle, and safety [1,2]. However, the performances of fuel cells are often impeded by the sluggish oxygen reduction reaction (ORR) at the cathode side. Platinum (Pt)-based materials have served as the most promising catalyst for the ORR, but they still suffer from many critical issues such as high cost, susceptibility to CO_2 poisoning and methanol crossover, and poor long-term stability [3,4]. Hitherto, enormous efforts have been devoted to developing non-precious metal or metal-free electrocatalysts for ORRs with high performance [3,5]. Among various candidates, nitrogen-doped (n-doped) graphene has emerged as a promising alternative to conventional Pt-based electrocatalysts, due to its unique advantages including low-cost, high selectivity, good electrocatalytic activity, and excellent long-term stability [3,6,7]. The facile generation of strong charge polarization between nitrogen atoms (x = 3.04) and carbon atoms (x = 2.55) greatly increases the ORR activity of n-doped graphene [8]. Once incorporated into the graphitic network, nitrogen atoms often possess three distinct configurations of pyridinic N, pyrrolic N, or graphitic N (or quaternary N) [9]. However, other specific arrangements of nitrogen atoms, including imine and pyrazine groups, can also be introduced into graphene structures to afford high-quality n-doped graphene for the ORR [10,11]. In addition, n-doped graphene electrocatalysts usually exhibit good ORR performance in alkaline electrolytes, while their activities are inferior in acidic media [12,13]. This result can be attributed to the facile conversion of active nitrogen species

into inactive ones, or the domination of less efficient two-electron process involved with intermediates during the ORR process of n-doped graphene in an acidic environment [14,15].

Despite these recent progresses, further enhancement in the ORR activity of n-doped graphene is highly demanding for large-scale commercialization. For example, the co-doping of transition metals into n-doped graphene can trigger a marked improvement in the overall ORR performance [16]. The additional doping of n-doped graphene with transition metals can induce not only the sharp increase in active sites but also facile intramolecular charge transfer between metal-bound nitrogen atoms [17]. However, complicated processes and harsh conditions at elevated temperatures are often required to prepare these multi-component n-doped graphene-based electrocatalysts [18]. Therefore, a simple but efficient approach, such as complex formation between transition metal ions and nitrogen-containing ligands on graphene structure [19], is strongly recommended for the development of high performance n-doped graphene-based electrocatalysts for the ORR.

Herein, we demonstrate the synthesis of terpyridine-containing imine-rich graphene (IrGO-Tpy) using an acid-catalyzed dehydration reaction between graphene oxide (GO) and 4′-(aminophenyl)-2,2′:6′2″-terpyridine (Figure 1). Owing to the efficient incorporation of imine linkages and terpyridine moieties into the graphene network, IrGO-Tpy displays promising electrocatalytic activity for the ORR with good selectivity, high resistance to methanol crossover, and excellent long-term stability. Moreover, the introduction of cobalt ions (Co^{2+}) into the structure of IrGo-Tpy through the existing terpyridine-mediated complexation [20,21] affords IrGO-Tpy-Co (Figure 1), which further enhances the ORR activity in an alkaline electrolyte. Therefore, the simple but efficient approach developed in this study provides not only a versatile technique to synthesize high-performance graphene-based electrocatalysts but also in-depth structure–property relationships for various applications.

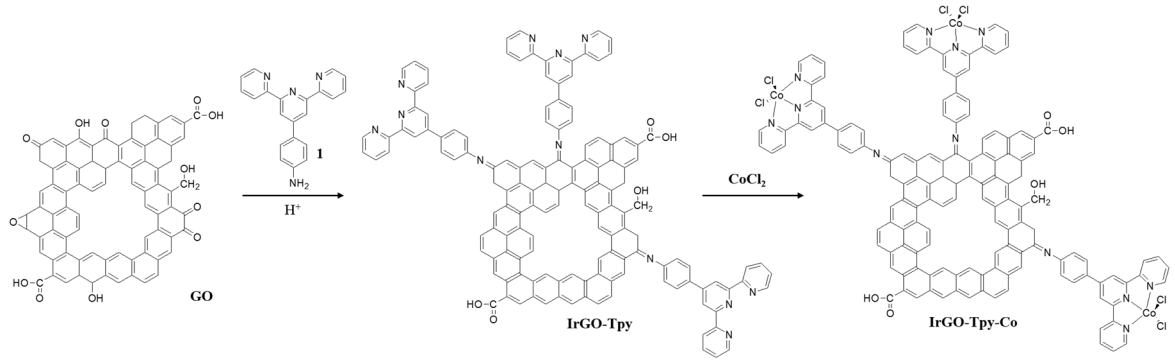

Figure 1. Synthesis of terpyridine-containing imine-rich graphene (IrGO-Tpy) and the related Co(II) complex (IrGO-Tpy-Co).

2. Results

2.1. Synthesis and Characterization

As schematically shown in Figure 1, IrGO-Tpy was prepared by an acid-catalyzed dehydration reaction between GO and 4′-(aminophenyl)-2,2′:6′2″-terpyridine. The facile condensation reaction between monoketones (-C=O) and primary amines ($-NH_2$) yielded typical imine (-C=N-) linkages in IrGO-Tpy. The elemental analysis (EA) data clearly show the compositional changes during the reactions. As summarized in Table S1, the pristine graphite possesses carbon atoms (98.74 wt%) as the main constituent, while a large population of oxygen atoms (42.10 wt%) with a concomitant decrease in carbon content (from 98.74 to 53.19 wt%) was observed in GO. This significant structural change is caused by the generation of various oxygenated functional groups such as hydroxyl, epoxy, and carboxylic groups during the severe oxidation process. Furthermore, additional compositional changes, including a sharp increase in nitrogen content (6.45 wt%) and a significant reduction of oxygen content (from 42.10 to 11.54 wt%) occurred after the acid-catalyzed dehydration

reaction between GO and 4′-(aminophenyl)-2,2′:6′2″-terpyridine. These results are consistent with the synthetic route to IrGO-Tpy shown in Figure 1.

Fourier transform infrared (FT-IR) spectra were measured to verify the structural changes during reaction, and the results are shown in Figure 2a. In comparison with the featureless spectrum of pristine graphite, that of GO exhibited several peaks characteristic of various oxygenated functionalities. However, IrGO-Tpy displayed two major characteristic peaks at 1576 and 1200 cm^{-1}, which are related to the in-plain vibrations of aromatic C=C sp^2 hybridized carbon and stretching modes of C=N, respectively [11]. In addition, the oxygenated peaks observed in GO decreased after its conversion to IrGO-Tpy, because of the efficient intramolecular and intermolecular acid-catalyzed dehydration reactions [22]. Thermogravimetric analysis (TGA) was also conducted in air, and the results are shown in Figure 2b. Pristine graphite was stable up to 600 °C, but GO displayed a noticeable weight loss near 200 °C because of the presence of numerous oxygenated functional groups. On the other hand, greatly improved thermal stability was observed for IrGO-Tpy, which can be attributed to the efficient removal of oxygenated moieties, as well as the formation of imine linkages during the acid-catalyzed dehydration reactions. Therefore, the obtained results from FT-IR and TGA measurements strongly support the proposed scheme in Figure 1.

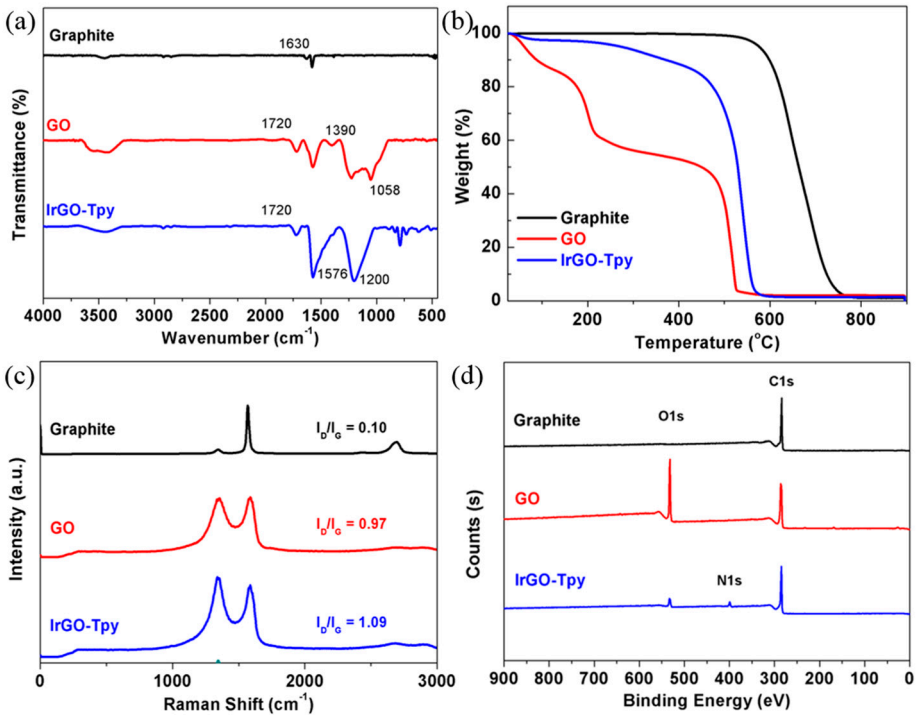

Figure 2. (**a**) FT-IR spectra, (**b**) TGA thermograms in air, (**c**) Raman spectra with I_D/I_G ratios, (**d**) XPS survey spectra of graphite, graphene oxide (GO), and IrGO-Tpy.

As shown in Figure 2c, the Raman spectrum of pristine graphite contains G and 2D bands at 1567 and 2685 cm^{-1}, respectively, with a negligible I_D/I_G ratio. However, a broad and strong D band at 1352 cm^{-1} with a high I_D/I_G ratio of 0.97 was obtained from that of GO, because of the size reduction in the in-plane sp^2 domains, and the large structural distortion induced by the harsh oxidation process. The spectrum of IrGO-Tpy also contains a strong D band, but its I_D/I_G ratio is further increased to 1.09. Similar to other n-doped graphenes [23,24], the incorporation of iminic nitrogen into the graphene structure can cause large topological defects or distortions. In addition, the power X-ray diffraction patterns (XRD) of all samples were collected, and the results are shown in Figure S1. As expected, a strong [002] peak at 2θ = 26.5° (*d*-spacing of 0.33 nm) was obtained from pristine graphite, whereas GO showed a broad peak at 2θ = 11.0° (*d*-spacing of 0.80 nm). The large lattice expansion caused by

diverse oxygenated functional groups can induce a sharp increase in the *d*-spacing of GO. Interestingly, the XRD peak of IrGO-Tpy recovered, moving to 2θ = 24.5° (*d*-spacing of 0.35 nm), which clearly reveals the efficient restoration of the graphitic structure during acid-catalyzed dehydration reaction. For further elucidation of compositional changes during reaction, X-ray photoelectron spectroscopy (XPS) measurements were conducted, and the results are shown in Figure 2d. In contrast to the pristine graphite used as a starting material, GO exhibited strong C 1s and O 1s peaks around 284 and 530 eV, respectively, arising from the generation of various oxygenated groups. Furthermore, the spectrum of IrGO-Tpy showed a sharp additional N 1s peak at around 400 eV with a noticeable reduction in the intensity of the O 1s peak. This result indicates the successful introduction of nitrogen atoms via the acid catalyzed dehydration reaction. Thus, the structure proposed in Figure 1 was fairly confirmed by Raman, XRD, and XPS measurements.

To investigate the morphology and microstructure of IrGO-Tpy, field emission scanning electron (FE-SEM), transmission electron microscopy (TEM), and surface area measurements were conducted. As shown in Figure 3a, large clusters of densely packed thin sheets were observed in the SEM image of GO, whereas that of IrGO-Tpy displayed wrinkled paper-like structures with a high electron transparency (Figure 3b). The low magnification TEM image of IrGO-Tpy also revealed similar crumpled film-like morphologies (Figure 3c). In addition, high-magnification TEM images of the edge and basal areas showed highly crystalline structures with the corresponding symmetric hexagonal selected area electron diffraction (SAED) patterns (Figure 3d,e), an indication of the efficient restoration of the graphene network during the acid-catalyzed dehydration reaction. Finally, the surface areas of GO and IrGO-Tpy were measured by the Brunauer–Emmett–Teller (BET) method, and the calculated values were 24.86 and 30.80 m^2 g^{-1}, respectively. The surface area of IrGO-Tpy is relatively smaller than those of other n-doped graphenes [25,26], due to the significant restacking of IrGO-Tpy layers through the strong attractive forces between them [27].

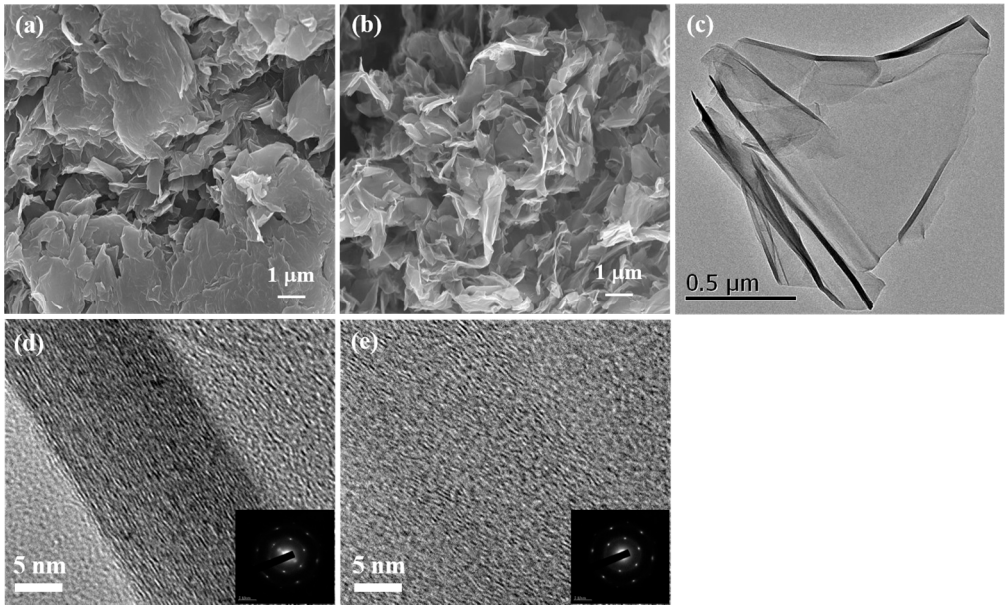

Figure 3. SEM images of (**a**) GO and (**b**) IrGO-Tpy; TEM images of IrGO-Tpy (**c**) at low-magnification and (**d**) at high-magnification on the edges with selected area electron diffraction (SAED) pattern. (**e**) High-magnification TEM images of the basal area with selected area electron diffraction (SAED) pattern.

Owing to the existence of terpyridine groups in IrGO-Tpy, various transition metal ions can be incorporated into its structure via complexation [17,28]. Among numerous candidates, Co^{2+} was selected, because carbon-based electrocatalytst with nitrogen-coordinated cobalt complexes usually exhibit superior electrocatalytic activities for the ORR [29,30]. The addition of Co^{2+} into

IrGO-Tpy readily led to the formation of cobalt–nitrogen co-doped graphene-based materials, denoted IrGO-Tpy-Co (Figure 1). As shown in Figure 4a, the XPS survey spectrum of IrGO-Tpy-Co clearly contains a Co 2p peak as well as peaks corresponding to oxygen, nitrogen, carbon, and chlorine. The related elemental compositions obtained from the XPS analysis are summarized in Table S2. In addition, the high-resolution Co 2p spectra displayed two main peaks at 781.5 and 796.8 eV for Co $2p_{3/2}$ and Co $2p_{1/2}$, respectively, with two corresponding satellite peaks at 786.3 and 803.5 eV, respectively (Figure 4a, inset). These results indicate the presence of Co^{2+} in IrGO-Tpy-Co [31,32]. Furthermore, the high-resolution N 1s spectra indicate the complexation of Co^{2+} ions with terpyridine moieties in IrGO-Tpy. As shown in Figure 4b (upper), the spectrum of IrGO-Tpy contains two main peaks at 398.6 and 399.9 eV, corresponding to pyridine-N and imine-N, respectively [27]. In addition, the relative percentages of pyridine-N (69.9%) and imine-N (30.1%) were calculated from the high-resolution XPS N 1s spectra, which agrees well with the chemical structure of 4′-(aminophenyl)-2,2′:6′2″-terpyridine used in this study. However, noticeable intensity enhancements in the higher binding energy region were observed for IrGO-Tpy-Co (Figure 4b (lower)), which agrees well with the typical N 1s peak shifts before and after metal complexation [33]. Once again, XPS analyses confirm the proposed structures and compositions of IrGO-Tpy-Co shown in Figure 1.

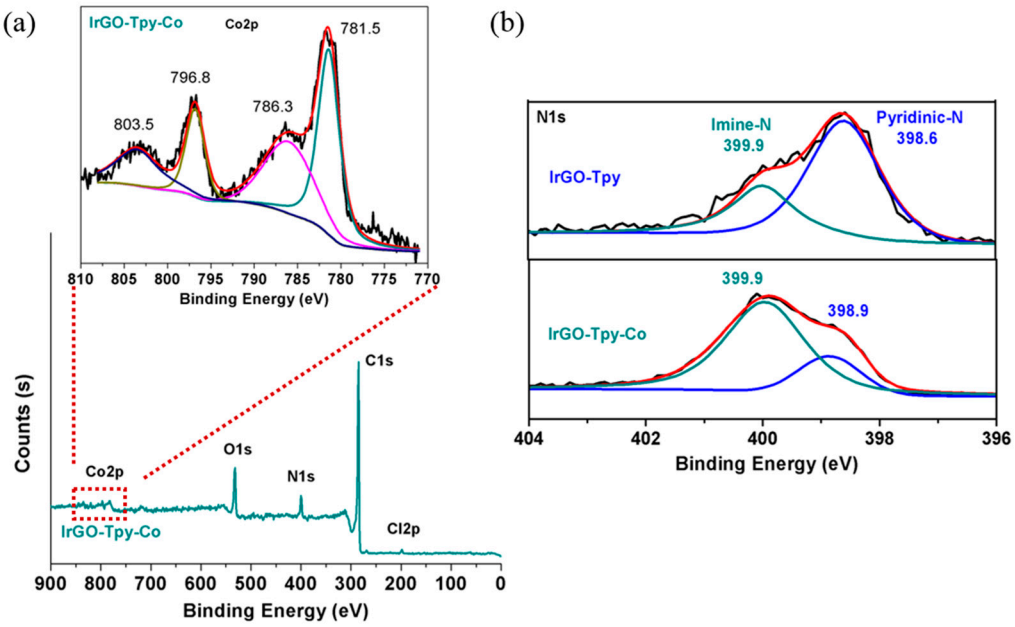

Figure 4. (**a**) XPS survey spectrum of IrGO-Tpy-Co, (inset) high-resolution Co 2p XPS spectrum of IrGo-Tpy-Co, and (**b**) N 1s XPS spectra of IrGO-Tpy (upper) and IrGO-Tpy-Co (lower).

2.2. Electrochemical and ORR Characteristics

The electrocatalytic activities of IrGO-Tpy and IrGO-Tpy-Co for the ORR were investigated using cyclovoltametric (CV) measurements in N_2- and O_2-saturated 0.1 M KOH electrolyte. As shown in Figure 5a,b, the CV curves of IrGO-Tpy and IrGO-Tpy-Co, respectively, show an apparent ORR peak near −0.20 V with an enhanced voltammetric current in the O_2-saturated electrolyte. In contrast, almost featureless smooth curves were observed in the corresponding N_2-saturated conditions, which reveals their profound electrocatalytic selectivity toward the ORR. For further investigation of the ORR characteristics of the samples, linear sweep voltammetry (LSV) measurements were carried out using a rotating ring disk electrode (RRDE) in O_2-saturated 0.1 M KOH electrolyte. As shown in Figure 5c, IrGO-Tpy-Co exhibited better ORR performances than those of IrGO-Tpy at a rotation speed of 1600 rpm. In particular, the onset potential and current density at −0.6 V of IrGO-Tpy were restricted to −0.18 V and −2.71 mA/cm^2, respectively, while those of IrGO-Tpy-Co were shifted to −0.11 V and

-3.80 mA/cm^2, respectively (Table S3). Although the onset potential and current density of IrGO-Tpy-Co are still lower than those of Pt/C (0.01 V and -5.18 mA/cm^2, respectively), these results demonstrate the significant contributions of complexation between Co^{2+} ion and terpyridine for facilitating the ORR. LSV curves of IrGO-Tpy-Co at different rotation speeds (625–2500 rpm) were also measured to analyze the ORR kinetics. The current densities of IrGO-Tpy-Co were found to be proportional to the rotating speeds, whereas the related onset potentials were almost identical (Figure 5d). Moreover, a good linear correlation between j^{-1} and $\omega^{-1/2}$ at -0.5 V was observed from the well-known Koutecky–Levich (K-L) plots of all samples [34], implying first-order ORR reactions kinetics (Figure 5e) [24]. As one of the most important kinetic parameters in the ORR process, the electron transfer number (n) can be calculated by either the K-L equation or the relevant equation using the ring and disk currents of RRDE measurement (see Equations (S1)–(S3) in the Supplementary Materials). As shown in Figure 5f and summarized in Table S3, the n values of IrGO-Tpy-Co obtained from RRDE voltammograms were much higher than those of IrGO-Tpy at all applied voltages. Although, the n values of IrGO-Tpy were limited to 3.0, those of IrGO-Tpy-Co were larger (3.6), indicating that the ORR process was close to an ideal four electron pathway ($n = 4$). As expected, the n values of Pt/C are close to 4.0 in all applied potentials (Figure 5f). In addition, the n values of all samples obtained from K-L equation agree well with those determined from RRDE voltammograms (Table S4). Furthermore, the yields of hydrogen peroxide (HO_2^-) during ORR were calculated from the relevant equation (see Equation (S4) in the Supplementary Materials) and the results were shown in Figure S2. The commercial Pt/C displayed negligible HO_2^- generation, while HO_2^- yield increases sharply in the order of IrGO-Tpy-Co < IrGO-Tpy. These clear enhancements in the ORR performances of IrGO-Tpy-Co can be attributed to the increased density of active sites and facile intramolecular charge transfer caused by complexation between Co^{2+} ions on terpyridine moieties in IrGO-Tpy.

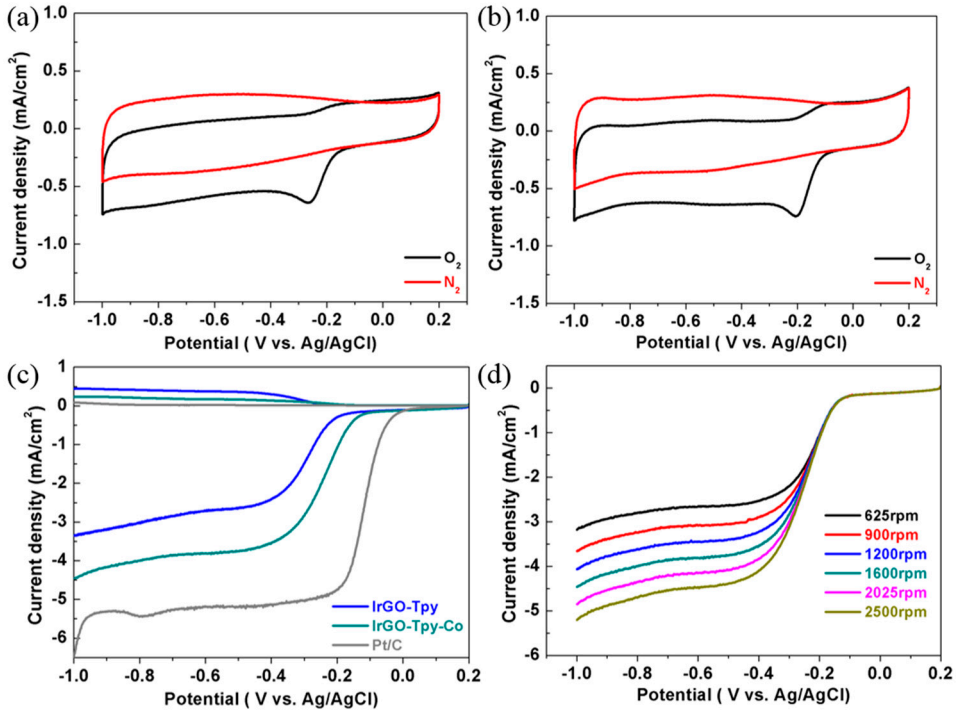

Figure 5. *Cont.*

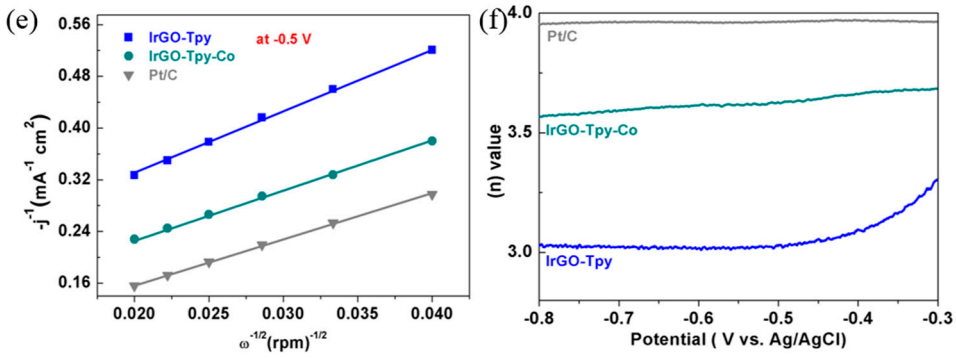

Figure 5. CV curves of (**a**) IrGO-Tpy and (**b**) IrGO-Tpy-Co in O_2- and N_2-saturated 0.1 M KOH solution at a scan rate of 10 mV/s, (**c**) RRDE voltammograms of all samples at a rotation speed of 1600 rpm, (**d**) linear sweep voltammetry (LSV) curves of IrGO-Tpy-Co at different rotation speeds (from 625 to 2500 rpm), (**e**) K-L plots of all samples obtained from LSV curves at −0.5 V, and (**f**) electron transfer number (*n*) of all samples calculated from RRDE voltammograms. Ag/AgCl (saturated KCl filled) was used as a reference electrode for all electrochemical measurements.

Long-term durability tests were carried out using chronoamperometric measurements at −0.40 V in O_2-saturated 0.1 M KOH electrolyte at a rotation rate of 1600 rpm. As shown in Figure 6a, 87.8% and 92.2% of initial currents were maintained by IrGO-Tpy and IrGO-Tpy-Co, respectively, even after 10,000 s, whereas the commercial Pt/C exhibited a great reduction of initial current (69%) under the same conditions. Furthermore, IrGO-Tpy and IrGO-Tpy-Co showed outstanding tolerance to methanol crossover. Once methanol had been added to electrolyte at around 360 s, an abrupt drop in the current density was observed from the Pt/C electrode, while no discernable changes in the current density were detected from IrGO-Tpy and IrGO-Tpy-Co upon the addition of methanol (Figure 6b).

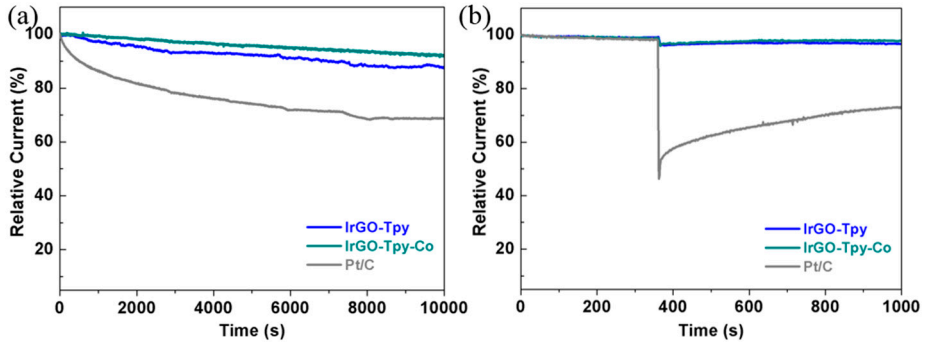

Figure 6. (**a**) Durability tests for IrGO-Tpy, IrGO-Tpy-Co, and Pt/C at a rotation rate of 1600 rpm in O_2-saturated 0.1 M KOH solution, and (**b**) current–time (j-t) ORR chronoamperometric responses of IrGO-Tpy, IrGO-Tpy-Co, and Pt/C upon the addition of 3 M methanol at around 360 s.

3. Materials and Methods

3.1. Synthesis of IrGO-Tpy and IrGO-Tpy-Co

4′-(Aminophenyl)-2,2′:6′2″-terpyridine (1) and GO were prepared according to previously reported methods [35,36]. For the synthesis of IrGO-Tpy, 0.60 g of GO was firstly dispersed in 300 mL of dimethylformamide (DMF) using sonication, and an acetic acid (10 mL) catalyst and amine-terminated terpyridine (1, 0.20 g) were then added consecutively. The mixture was stirred overnight at 120 °C. Once the reaction had completed, IrGO-Tpy was collected by filtration using a 0.45 μm PTFE membrane and further purified via continuous Soxhlet extraction with water, tetrahydrofuran (THF),

and methanol. Finally, IrGO-Tpy was obtained as a black powder (0.32 g) after vacuum-drying at 50 °C. For the synthesis of IrGO-Tpy-Co, 120 mg of IrGO-Tpy was dispersed in 150 mL DMF, and a 5 mL DMF solution of $CoCl_2 \cdot 6H_2O$ (0.01 M) was slowly added to form the cobalt complex. After sonication for 2 min, the mixture was stirred for 3 h to complete complexation. IrGO-Tpy-Co was collected by filtration and washed with plenty of DMF, followed by drying in a vacuum oven.

3.2. Characterization and Electrochemical Study

EA was conducted using a Thermo Scientific Flash 2000 (Thermo Fisher, Waltham, MA, USA). FT-IR spectra were collected using a Perkin-Elmer Spectrometer 100 with a KBr Pellet (Perkin Elmer Company, Waltham, MA, USA). TGA measurements were carried out using a TA Q200 at a heating rate of 10 °C/min in air (Perkin Elmer Company, Waltham, MA, USA). Raman spectra and XRD patterns were recorded on a confocal Raman microscope (Alpha 200S, WITec, Ulm, Germany) and a Rigaku D/MAZX 2500V/PC (Rigaku, Tokyo, Japan), respectively. XPS measurements were made with a Thermo Fisher K-alpha spectrometer (Thermo Fisher, Waltham, MA, USA). FE-SEM and TEM were conducted using an FEI Nanonova 230 (FEI, Hillsboro, OR, USA) and a JEOL JEM-2100F microscope (JEOL, Tokyo, Japan), respectively. The surface area was determined by the Brunauer–Emmett–Teller (BET) method using a Micromeritics ASAP 2504N (Micromeritics, Norcross, GA, USA). CV measurements were carried out using a PARSTAT multichannel potentiostat (AMETEK, Berwyn, PA, USA). LSV with a rotating ring disk electrode (RRDE, glassy carbon disk with a 4 mm diameter and a Pt ring with 5 mm/7 mm inner/outer diameters) was conducted using an RRDE-3A electrode rotator (BAS Inc., Tokyo, Japan) connected to a potentiostat. For the preparation of catalyst ink, 3 mg of sample was well dispersed in a mixed solution of *N*-methyl-2-pyrrolidone (285 μL) and a 3% Nafion ethanol solution (15 μL) using sonication. The catalyst loading levels on the GC electrode were adjusted to 0.20 mg/cm^2, and the rotating speeds varied from 625 to 2500 rpm. A typical three-electrode cell was used for the CV and RRDE analyses, in which a glassy carbon electrode coated with the sample, a platinum wire, and Ag/AgCl (saturated KCl filled) were used as working, counter, and reference electrodes, respectively. A 0.1 M aqueous solution of KOH was used as an electrolyte for electrochemical study. N_2 and O_2 gases were bubbled into the KOH solution to produce oxygen-free and oxygen-saturated conditions.

4. Conclusions

We report here a facile synthetic approach to prepare terpyridine-containing imine-rich graphene (IrGO-Tpy) via an acid-catalyzed dehydration reaction between GO and 4′-(aminophenyl)-2,2′:6′2″-terpyridine. The unique features of IrGO-Tpy, including the incorporation of imine-N and pyridine-N, and the good structural restoration of the graphene network, were clearly demonstrated by numerous spectroscopic and microscopic analyses. In addition, Co^{2+} was incorporated into IrGO-Tpy through terpyridine-meditated complexation, affording the formation of cobalt-nitrogen co-doped graphene-based material, denoted here as IrGO-Tpy-Co. Owing to their unique structures and compositions, IrGO-Tpy and IrGO-Tpy-Co exhibited several adventurous ORR features, such as good selectivity to the 4-electron pathway, superior long-term stability, and excellent tolerance to methanol crossover. Interestingly, a great enhancement in electrocatalytic ORR performance was observed for IrGO-Tpy-Co in comparison to that of IrGO-Tpy, implying the significant contribution of the cobalt–terpyridine complexation in facilitating the ORR. Therefore, the results obtained from this study not only pave the way for the development of high-performance ORR electrocatalysts but also offer meaningful insights into the structure–property relationships of metal–nitrogen co-doped graphene-based materials.

Supplementary Materials: The following are available online at www.mdpi.com/2073-4344/7/11/338/s1. Figure S1: XRD diffraction patterns of graphite, GO, and IrGO-Tpy with *d*-spacing; Figure S2: Peroxide percentages of IrGo-Tpy, IrGO-Tpy-Co, Pt/C; Table S1: Elemental analyses of graphite, GO, and IrGo-Tpy; Table S2: Elemental compositions of IrGo-Tpy and IrGO-Tpy-Co; Table S3: Onset potentials and current densities of samples; Table S4: Electron transferred numbers (*n*) of all samples from K-L plots and RRDE measurements.

Acknowledgments: This research was supported by basic science research grants (2015R1D1A1A01057410) from the National Research Foundation (NRF) of Korea, and the Korea Institute of Energy Technology Evaluation and Planning (KETEP) and the Ministry of Trade, Industry & Energy (MOTIE) of Korea (20174010201460).

Author Contributions: Min Seok Lee and Dong Wook Chang designed the experiments; Min Seok Lee and Mun Ho Yang performed the experiments; Jong S. Park and Dong Wook Chang analyzed the data; Min Seok Lee and Dong Wook Chang wrote the paper.

Conflicts of Interest: The authors declare no conflict of interest.

References

1. Porter, N.S.; Wu, H.; Quan, Z.; Fang, J. Shape-control and electrocatalytic activity-enhancement of pt-based bimetallic nanocrystals. *Acc. Chem. Res.* **2013**, *46*, 1867–1877. [CrossRef] [PubMed]
2. Acres, G.J. Recent advances in fuel cell technology and its applications. *J. Power Sources* **2001**, *100*, 60–66. [CrossRef]
3. Dai, L.; Xue, Y.; Qu, L.; Choi, H.-J.; Baek, J.-B. Metal-free catalysts for oxygen reduction reaction. *Chem. Rev.* **2015**, *115*, 4823–4892. [CrossRef] [PubMed]
4. Sealy, C. The problem with platinum. *Mater. Today* **2008**, *11*, 65–68. [CrossRef]
5. Chen, Z.; Higgins, D.; Yu, A.; Zhang, L.; Zhang, J. A review on non-precious metal electrocatalysts for pem fuel cells. *Energy Environ. Sci.* **2011**, *4*, 3167–3192. [CrossRef]
6. Tong, X.; Wei, Q.; Zhan, X.; Zhang, G.; Sun, S. The new graphene family materials: Synthesis and applications in oxygen reduction reaction. *Catalysts* **2017**, *7*, 1. [CrossRef]
7. Wei, Q.; Tong, X.; Zhang, G.; Qiao, J.; Gong, Q.; Sun, S. Nitrogen-doped carbon nanotube and graphene materials for oxygen reduction reactions. *Catalysts* **2015**, *5*, 1574–1602. [CrossRef]
8. Jeon, I.Y.; Zhang, S.; Zhang, L.; Choi, H.J.; Seo, J.M.; Xia, Z.; Dai, L.; Baek, J.B. Edge-selectively sulfurized graphene nanoplatelets as efficient metal-free electrocatalysts for oxygen reduction reaction: The electron spin effect. *Adv. Mater.* **2013**, *25*, 6138–6145. [CrossRef] [PubMed]
9. Wang, H.; Maiyalagan, T.; Wang, X. Review on recent progress in nitrogen-doped graphene: Synthesis, characterization, and its potential applications. *ACS Catal.* **2012**, *2*, 781–794. [CrossRef]
10. Lee, M.S.; Whang, D.R.; Choi, H.-J.; Yang, M.H.; Kim, B.-G.; Baek, J.-B.; Chang, D.W. A facile approach to tailoring electrocatalytic activities of imine-rich nitrogen-doped graphene for oxygen reduction reaction. *Carbon* **2017**, *122*, 515–523. [CrossRef]
11. Chang, D.W.; Choi, H.-J.; Baek, J.-B. Wet-chemical nitrogen-doping of graphene nanoplatelets as electrocatalysts for the oxygen reduction reaction. *J. Mater. Chem.* **2015**, *3*, 7659–7665. [CrossRef]
12. Zhan, Y.; Huang, J.; Lin, Z.; Yu, X.; Zeng, D.; Zhang, X.; Xie, F.; Zhang, W.; Chen, J.; Meng, H. Iodine/nitrogen co-doped graphene as metal free catalyst for oxygen reduction reaction. *Carbon* **2015**, *95*, 930–939. [CrossRef]
13. Choi, C.H.; Park, S.H.; Woo, S.I. Binary and ternary doping of nitrogen, boron, and phosphorus into carbon for enhancing electrochemical oxygen reduction activity. *ACS Nano* **2012**, *6*, 7084–7091. [CrossRef] [PubMed]
14. Muthukrishnan, A.; Nabae, Y.; Okajima, T.; Ohsaka, T. Kinetic approach to investigate the mechanistic pathways of oxygen reduction reaction on Fe-containing n-doped carbon catalysts. *ACS Catal.* **2015**, *5*, 5194–5202. [CrossRef]
15. Bai, J.; Zhu, Q.; Lv, Z.; Dong, H.; Yu, J.; Dong, L. Nitrogen-doped graphene as catalysts and catalyst supports for oxygen reduction in both acidic and alkaline solutions. *Int. J. Hydrogen Energy* **2013**, *38*, 1413–1418. [CrossRef]
16. Wu, G.; Zelenay, P. Nanostructured nonprecious metal catalysts for oxygen reduction reaction. *Acc. Chem. Res.* **2013**, *46*, 1878–1889. [CrossRef] [PubMed]
17. Sauvage, J.P.; Collin, J.P.; Chambron, J.C.; Guillerez, S.; Coudret, C.; Balzani, V.; Barigelletti, F.; De Cola, L.; Flamigni, L. Ruthenium(II) and osmium(II) bis (terpyridine) complexes in covalently-linked multicomponent systems: Synthesis, electrochemical behavior, absorption spectra, and photochemical and photophysical properties. *Chem. Rev.* **1994**, *94*, 993–1019. [CrossRef]
18. Wu, G.; Santandreu, A.; Kellogg, W.; Gupta, S.; Ogoke, O.; Zhang, H.; Wang, H.-L.; Dai, L. Carbon nanocomposite catalysts for oxygen reduction and evolution reactions: From nitrogen doping to transition-metal addition. *Nano Energy* **2016**, *29*, 83–110. [CrossRef]

19. Song, S.; Xue, Y.; Feng, L.; Elbatal, H.; Wang, P.; Moorefield, C.N.; Newkome, G.R.; Dai, L. Reversible self-assembly of terpyridine-functionalized graphene oxide for energy conversion. *Angew. Chem. Int. Ed.* **2014**, *53*, 1415–1419. [CrossRef] [PubMed]
20. Andres, P.R.; Schubert, U.S. New functional polymers and materials based on 2, 2′: 6′, 2″-terpyridine metal complexes. *Adv. Mater.* **2004**, *16*, 1043–1068. [CrossRef]
21. Schubert, U.S.; Alexeev, A.; Andres, P.R. Terpyridine-functionalized tentagel microbeads: Synthesis, metal chelation and first sequential complexation. *Macromol. Mater. Eng.* **2003**, *288*, 852–860. [CrossRef]
22. Chang, D.W.; Lee, E.K.; Park, E.Y.; Yu, H.; Choi, H.-J.; Jeon, I.-Y.; Sohn, G.-J.; Shin, D.; Park, N.; Oh, J.H. Nitrogen-doped graphene nanoplatelets from simple solution edge-functionalization for n-type field-effect transistors. *J. Am. Chem. Soc.* **2013**, *135*, 8981–8988. [CrossRef] [PubMed]
23. Wei, D.; Liu, Y.; Wang, Y.; Zhang, H.; Huang, L.; Yu, G. Synthesis of n-doped graphene by chemical vapor deposition and its electrical properties. *Nano Lett.* **2009**, *9*, 1752–1758. [CrossRef] [PubMed]
24. Wu, J.; Zhang, D.; Wang, Y.; Hou, B. Electrocatalytic activity of nitrogen-doped graphene synthesized via a one-pot hydrothermal process towards oxygen reduction reaction. *J. Power Sources* **2013**, *227*, 185–190. [CrossRef]
25. Yang, J.; Jo, M.R.; Kang, M.; Huh, Y.S.; Jung, H.; Kang, Y.-M. Rapid and controllable synthesis of nitrogen doped reduced graphene oxide using microwave-assisted hydrothermal reaction for high power-density supercapacitors. *Carbon* **2014**, *73*, 106–113. [CrossRef]
26. Zhang, H.; Kuila, T.; Kim, N.H.; Yu, D.S.; Lee, J.H. Simultaneous reduction, exfoliation, and nitrogen doping of graphene oxide via a hydrothermal reaction for energy storage electrode materials. *Carbon* **2014**, *69*, 66–78. [CrossRef]
27. Lee, M.S.; Choi, H.-J.; Baek, J.-B.; Chang, D.W. Simple solution-based synthesis of pyridinic-rich nitrogen-doped graphene nanoplatelets for supercapacitors. *Appl. Energy* **2017**, *195*, 1071–1078. [CrossRef]
28. Schubert, U.S.; Eschbaumer, C. Macromolecules containing bipyridine and terpyridine metal complexes: Towards metallosupramolecular polymers. *Angew. Chem. Int. Ed.* **2002**, *41*, 2892–2926. [CrossRef]
29. McGuire, R., Jr.; Dogutan, D.K.; Teets, T.S.; Suntivich, J.; Shao-Horn, Y.; Nocera, D.G. Oxygen reduction reactivity of cobalt(II) hangman porphyrins. *Chem. Sci.* **2010**, *1*, 411–414. [CrossRef]
30. Tang, H.; Yin, H.; Wang, J.; Yang, N.; Wang, D.; Tang, Z. Molecular architecture of cobalt porphyrin multilayers on reduced graphene oxide sheets for high-performance oxygen reduction reaction. *Angew. Chem. Int. Ed.* **2013**, *125*, 5695–5699. [CrossRef]
31. Yuvaraj, S.; Vignesh, R.H.; Vasylechko, L.; Lee, Y.; Selvan, R.K. Synthesis and electrochemical performance of Co_2TiO_4 and its core–shell structure of Co_2TiO_4@C as negative electrodes for li-ion batteries. *RSC Adv.* **2016**, *6*, 69016–69026. [CrossRef]
32. Jin, S.; Yang, G.; Song, H.; Cui, H.; Wang, C. Ultrathin hexagonal 2D Co_2GeO_4 nanosheets: Excellent Li-storage performance and ex situ investigation of electrochemical mechanism. *ACS Appl. Mater. Interfaces* **2015**, *7*, 24932–24943. [CrossRef] [PubMed]
33. Takada, K.; Sakamoto, R.; Yi, S.-T.; Katagiri, S.; Kambe, T.; Nishihara, H. Electrochromic bis (terpyridine) metal complex nanosheets. *J. Am. Chem. Soc.* **2015**, *137*, 4681–4689. [CrossRef] [PubMed]
34. Chen, Z.; Higgins, D.; Chen, Z. Nitrogen doped carbon nanotubes and their impact on the oxygen reduction reaction in fuel cells. *Carbon* **2010**, *48*, 3057–3065. [CrossRef]
35. Koohmareh, G.A.; Sharifi, M. Synthesis, characterization, and coordination behavior of copoly (styrene-maleimide) functionalized with terpyridine. *J. Appl. Polym. Sci.* **2010**, *116*, 179–183. [CrossRef]
36. Hummers, W.S., Jr.; Offeman, R.E. Preparation of graphitic oxide. *J. Am. Chem. Soc.* **1958**, *80*, 1339. [CrossRef]